Monthly Notices
of the
ROYAL ASTRONOMICAL SOCIETY

MNRAS **468,** 2333–2344 (2017)
Advance Access publication 2017 March 17

doi:10.1093/mnras/stx648

Ultraviolet spectroscopy of the blue supergiant SBW1: the remarkably weak wind of a SN 1987A analogue

Nathan Smith,[1]★ Jose H. Groh,[2] Kevin France[3] and Richard McCray[4]

[1]*Steward Observatory, University of Arizona, 933 N. Cherry Ave., Tucson, AZ 85721, USA*
[2]*Trinity College Dublin, The University if Dublin, Dublin 2, Ireland*
[3]*Laboratory for Atmospheric and Space Physics, University of Colorado, 600 UCB, Boulder, CO 80309, USA*
[4]*Department of Astronomy, University of California, Berkeley, CA 94720-3411, USA*

Accepted 2017 March 14. Received 2017 January 19; in original form 2016 June 10

ABSTRACT

The Galactic blue supergiant SBW1 with its circumstellar ring nebula represents the best known analogue of the progenitor of SN 1987A. High-resolution imaging has shown Hα and infrared structures arising in an ionized flow that partly fills the ring's interior. To constrain the influence of the stellar wind on this structure, we obtained an ultraviolet (UV) spectrum of the central star of SBW1 with the *Hubble Space Telescope* Cosmic Origins Spectrograph. The UV spectrum shows none of the typical wind signatures, indicating a very low mass-loss rate. Radiative transfer models suggest an extremely low rate below 10^{-10} M$_\odot$ yr^{-1}, although we find that cooling time-scales probably become comparable to (or longer than) the flow time below 10^{-8} M$_\odot$ yr^{-1}. We therefore adopt this latter value as a conservative upper limit. For the central star, the model yields $T_{\rm eff} = 21\,000 \pm 1000$ K, $\log(g_{\rm eff}) = 3.0$, $L \simeq 5 \times 10^4$ L$_\odot$, and roughly Solar composition except for enhanced N abundance. SBW1's very low mass-loss rate may hinder the wind's ability to shape its nebula and to shed angular momentum. The spin-down time-scale for magnetic breaking is more than 500 times longer than the age of the ring. This, combined with the star's slow rotation rate, constrains merger scenarios to form ring nebulae. The mass-loss rate is at least 10 times lower than expected from mass-loss recipes, without any account of clumping. The physical explanation for why SBW1's wind is so weak presents an interesting mystery.

Key words: binaries: general – circumstellar matter – stars: evolution – stars: massive – stars: mass loss – stars: winds, outflows.

1 INTRODUCTION

SN 1987A was the nearest supernova (SN) in modern times. Two surprising observations associated with SN 1987A (see the review by Arnett et al. 1989) were the identification of a blue supergiant (BSG) progenitor in pre-explosion images (Rousseau et al. 1978; Arnett 1987; Arnett et al. 1989; Walborn et al. 1989) and its very unusual triple-ring circumstellar nebula (Burrows et al. 1995; Crotts, Kunkel & Heathcote 1995). These two are intimately related, since the geometry of the nebula bears the imprint of mass-loss shaped by binary interaction and/or rapid rotation as the star evolved to its blue pre-SN state. The dynamical age of the nebula is only ∼20 000 yr (Meaburn, Bryce & Holloway 1995; Crotts & Heathcote 2000), so the nebular structures trace recent pre-SN mass-loss on a time-scale much shorter than core He burning and longer than C burning. The total mass of the ring is uncertain (due to an uncertain neutral fraction), but may be 0.1–1 M$_\odot$ (Fransson et al. 2015). An important unresolved question is whether or not close binary evolution was key in determining the progenitor's BSG state (mass transfer or merger, mass-loss, etc.). The ring nebula may therefore provide important clues to how and why the progenitor came to be a BSG.

Understanding the origin of the observed triple-ring structure has been difficult, however. Several early models showed that a faster BSG wind expanding into a previous slower red supergiant (RSG) wind with an equatorial density enhancement could yield an equatorial ring and bipolar structure (Luo & McCray 1991; Blondin & Lundqvist 1993; Martin & Arnett 1995; Collins et al. 1999). However, the pairs of polar rings around SN 1987A really are empty rings, rather than limb-brightened polar lobes or filled caps, and their origin has not been satisfactorily explained. It is difficult to understand the origin of the equatorial density enhancement in a RSG wind without invoking a binary (Collins et al. 1999). In subsequent studies, two different types of models have been proposed as plausible ways to form the nebula. A scenario involving a binary merger as a RSG and subsequent blueward evolution was proposed (Morris & Podsiadlowski 2007, 2009), and was suggested to account for the observed nebular structure. However, this specific

★ E-mail: nathans@as.arizona.edu

merger model predicts filled polar caps and relatively empty mid-latitudes in the nebula, whereas the observed nebula has no polar caps and may have some emission in the side walls of an hourglass structure. Moreover, the model requires that the merger product should be rotating very rapidly, which seems to be at odds with Galactic analogues. A somewhat different model involves rotating single-star evolution, where a massive star spins up as it contracts on a post-RSG blue loop, nearly reaching critical rotation and ejecting a ring (Chita et al. 2008). Then a bipolar wind from the rotating BSG expands into the RSG wind and ring, forming transient structures that may resemble the rings of SN 1987A (Chita et al. 2008). However, this model also requires a rapidly rotating BSG, inconsistent with observations of Galactic analogues. In either case, the strength of the BSG wind is a critical ingredient.

Radio observations of SN 1987A (or rather, the lack of detectable radio emission at early times) suggested that for the first 1000–1500 d after explosion, the blast wave was expanding relatively unimpeded through a very low density wind (Staveley-Smith et al. 1993). After about 1500 d, however, the radio emission brightened and the expansion speed slowed to only 3500 km s^{-1} (Gaensler et al. 1997, 2000; Zanardo et al. 2013). In order to reach the angular scale of the resolved radio emission when it turned on, the blast wave must have been expanding at about 35 000 km s^{-1} for those first 1500 d (Staveley-Smith et al. 1993). Chevalier & Dwarkadas (1995) suggested that after the initial free expansion through a rarefied wind with $\dot{M} = 7.5\times\ 10^{-8}\,M_{\odot}$ yr^{-1} or less, the blast wave slammed into a dense H II region that partly filled the ring's interior. In this model, the dense H II region was created by photoionization of the RSG wind by the BSG's ultraviolet (UV) radiation. This collision slowed the forward shock's expansion and caused the radio emission to brighten dramatically (Chevalier & Dwarkadas 1995).

Since the progenitor star Sk−69°202 is now dead, it is hard to improve our understanding of the connection between the star and its nebula. For this reason, nearby analogues of SN 1987A's progenitor – where the BSG has not yet exploded – become interesting and valuable. There are currently three well-studied analogues known in our Galaxy: (1) Sher 25 (Brandner et al. 1997; Smartt et al. 2002), which is significantly more luminous and has partial polar caps instead of rings, (2) HD 168625 (Smith 2007), which is a more luminous LBV candidate that does have polar rings, and (3) SBW1 (Smith, Bally & Walawender 2007) (discussed below).[1] An interesting recent result places important constraints on the formation of these rings: Taylor et al. (2014) monitored the central stars of all three Galactic analogues with high-resolution spectroscopy and did not find any radial velocity variations consistent with close massive binaries (the value of sin *i* is presumed from the resolved equatorial rings; if a binary system's orbit were significantly misaligned with these rings, then binary interaction would not help to explain them). Perhaps even more interesting, Taylor et al. (2014) found that all three BSG central stars have relatively *slow rotation speeds*. For SBW1, the rotation speed is only about 40 km s^{-1}. Such slow rotation may be quite problematic for some merger models that would predict a rapidly rotating BSG post-merger product – especially if the stellar wind in the BSG phase is very weak. We will return to this issue later in this paper.

Of these three Galactic analogues, SBW1 is currently the best known analogue to SN 1987A in terms of stellar properties and nebular structure. The ring around SBW1 was discovered by Smith et al. (2007) during a survey of the Carina Nebula, but two factors suggest that it is actually located several kpc *behind* the Carina Nebula and is seen there in projection. First, its positive radial velocity compared to expectations for Galactic rotation in that direction suggest that it is on the far side of the Sagittarius-Carina arm and outside the Solar circle. Secondly, its apparent magnitude and colour only match its spectral type and luminosity class (B1.5 Iab; Smith et al. 2007) if it is much more distant than the Carina Nebula. At a distance of 6–7 kpc, the stellar luminosity (0.5–1 $\times$ 10^5 L$_{\odot}$) as well as the size of the ring nebula ($r \simeq 0.2$ pc) make SBW1 a close match for SN 1987A.

Detailed analysis of the SBW1 nebula has provided interesting clues that may alter our ideas about the formation of the nebula around SN 1987A. *Hubble Space Telescope* (*HST*) images of SBW1 (Smith et al. 2013) show a pattern of clumps around the ring and a radial extent that closely resemble the spacing and size scale of spots in the ring of SN 1987A. The interior of the ring is filled with diffuse Hα emission, although the ring would probably appear much brighter relative to the interior if it were flash-ionized by a SN (Smith et al. 2013). A very interesting result is that high-resolution ground-based infrared (IR) images show that the interior of the ring is also partly filled with diffuse emission from warm dust. Since BSGs do not produce dust in their winds, this requires that the dust inside the ring was entrained from the ring itself. Smith et al. (2013) proposed that this structure arises because the inner surface of the dense and neutral equatorial ring is ionized by the central star, and that this triggers a dusty ionized photoevaporative flow that fills the interior of the ring. The ionized gas expands into the ring until it collides with the stellar wind; entrained dust piles up at this interface, producing the observed peaks of thermal-IR emission inside the ring (Smith et al. 2013). This simple ionized flow is able to dramatically influence the observed structure and dynamics of the nebula because the ring's expansion is slow (10–20 km s^{-1}), comparable to the sound speed of the ionized gas. This directly imaged structure around SBW1 appears to validate the picture of an H II region inside the ring of SN 1987A proposed by Chevalier & Dwarkadas (1995), which was deduced from the time evolution of the SN's radio emission. In this scenario, the main requirement is that the star ejected a thin, dense ring about 10^4 yr ago. While this might have occurred in post-RSG evolution to the blue (perhaps with a merger), a ring might also be ejected in a brief mass-transfer episode of a close binary or in an eruptive mass-loss event from a rotating star (e.g. Smith & Townsend 2007). A previous RSG phase is not necessarily required (Smith et al. 2007).

In order to test whether this proposed scenario actually works for the specific case of SBW1, we need to know the mass-loss rate of the wind from the central star, because this was an assumed parameter in our previous analysis (Smith et al. 2013). For this reason, we proposed to obtain UV spectra of the central star. Optical spectra are useful for constraining atmosphere/wind models as well, but the UV resonance lines are usually the most sensitive probes of the wind density and speed. Our new observations are discussed in Section 2, our analysis of the data including a comparison with radiative transfer models is presented in Section 3, and a discussion of the results and implications is given in Section 4.

2 OBSERVATIONS

In Cycle 20 (programme GO-12924), we used the Cosmic Origins Spectrograph (COS), onboard the *HST*, to observe the UV spectrum of the BSG star at the centre of the SBW1 ring nebula. We used

[1] Another possible member of the group is MN18, which is a similar BSG with a ring-like bipolar nebula (Gvaramadze et al. 2015), although this object has not yet been studied in as much detail as the others.

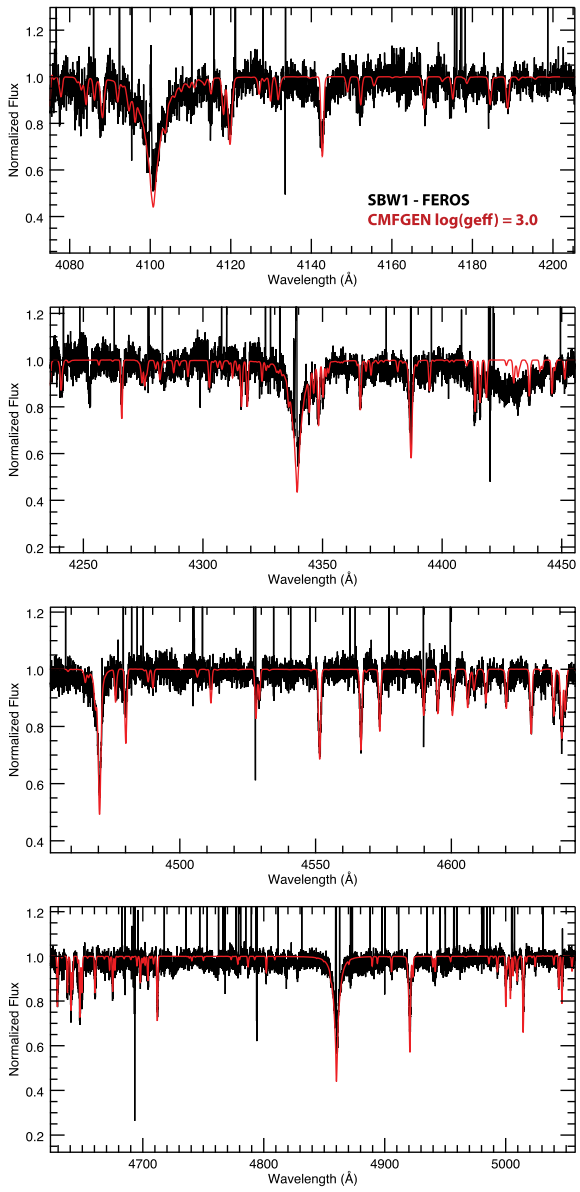

Figure 1. A blue-wavelength echelle spectrum of the central star of SBW1 (in black), obtained with the FEROS spectrograph and published previously by Taylor et al. (2014), compared to a CMFGEN model with the favoured value of $g_{\rm eff} = 3.0$ (in red). The broad feature at $\lambda \simeq 4430$ Å in the observed spectrum is due to absorption by a known diffuse interstellar band.

FUV mode in the G160M grating with central wavelengths of 1577 and 1600 Å. These two grating tilts were combined to fill the gap between the microchannel plate detector segments. The COS observations were taken on 2013 March 24. The resulting spectral coverage was 1384–1777 Å, with a spectral resolving power R of 16 000–18 000 (17–19 km s^{-1}). Across most of the spectrum. the total exposure time was 11.5 ks, although at the edges and middle of the wavelength range (corresponding to the COS detector gap that was filled), the effective exposure time dropped as low as ∼4 ks. The regions with this lower signal-to-noise ratio did not include important diagnostic lines like Si IV and C IV discussed below.

In our analysis below, we also include normalized visible-wavelength spectra of the central star. Fig. 1 shows a comparison between our CMFGEN model and an echelle spectrum of the star

Table 1. CMFGEN atomic model used in the analysis of SBW 1.

Ion	$N_{\rm S}$	$N_{\rm F}$	$N_{\rm T}$
H I	30	30	435
He I	69	69	1539
He II	22	30	905
C II	80	238	5538
C III	99	243	4571
C IV	64	64	5528
N I	44	44	885
N II	120	194	2390
N III	120	211	4284
O I	69	161	358
O II	54	123	1375
O III	88	170	1762
Na I	22	71	1550
Mg I	41	41	558
Mg II	18	45	358
Al II	31	31	848
Al III	21	65	1348
Si II	43	43	365
Si III	34	34	183
Si IV	33	33	92
Fe II	100	510	7501
Fe III	65	607	5482
Fe IV	58	272	3113
Fe V	25	168	1938
Ni II	29	204	2431
Ni III	28	220	2527
Ni IV	36	200	2337
Ni V	46	183	1524

Notes. For each species, an additional one-level ion corresponding to the highest ionization stage was included explicitly in the rate equations (i.e. C V for carbon, for instance), but is not shown above for brevity. The columns correspond to $N_{\rm S}$ = number of included superlevels, $N_{\rm F}$ = number of total energy levels and $N_{\rm T}$ = number of bound-bound transitions included for each ion.

at blue wavelengths obtained with the FEROS spectrograph and published previously (Taylor et al. 2014). In order to help further constrain the value of the effective gravity from the wings of Balmer lines, we also compare models to a high-resolution echelle spectrum of SBW1's Hα line published previously (Smith et al. 2007), discussed later.

3 CMFGEN MODELS

We use the radiative transfer code CMFGEN (Hillier & Miller 1998) to analyse the optical and UV spectrum of SBW1. CMFGEN self-consistently solves the radiative transfer in a stellar atmosphere and spherically symmetric, stationary wind. Line and continuum formation are calculated in the non-local thermodynamic equilibrium regime. Each model is defined by the effective temperature $T_{\rm eff}$ (evaluated at a Rosseland optical depth of 2/3), luminosity $L_\star$, effective gravity $g_{\rm eff}$, mass-loss rate $\dot{M}$, wind terminal velocity v_∞, velocity law, and chemical abundances. CMFGEN accounts for line blanketing, and we include the appropriate ionization stages of H, He, C, N, O, Si, Mg, Al, Fe and Ni in the analysis of SBW1. Table 1 summarizes the adopted atomic model. CMFGEN uses an ad hoc

Table 2. Stellar and wind parameters of SBW1 derived with CMFGEN. Some values have a range because of distance uncertainties. As discussed in the text, consistency favours values of $L = 5 \times 10^4$ L$_\odot$, log $Q_{\rm H} = 47.44$ s^{-1} and log $g_{\rm eff} = 3.0$.

Quantity	Value
Luminosity $L_\star$ (L$_\odot$)	$5.5(\pm1)\times 10^4$
Effective tempreature $T_{\rm eff}$ (K, at $\tau_{\rm Ross} = 2/3$)	$21\,000 \pm 1000$
Log H ionizing photon flux $Q_{\rm H}$ (s^{-1})	47.19-47.49
Log effective gravity (cm s^{-2})	3.0 ± 0.1
Wind terminal velocity (km s^{-1})	300 (assumed)
Mass-loss rate (M$_\odot$ yr^{-1})	$<1.0 \times 10^{-10}$
He/H (by number)	0.1
12 + log C/H (number)	7.92 ±0.3
12 + log N/H (number)	8.13 ±0.3
12 + log O/H (number)	8.69 ±0.3
log N/C − log N$_\odot$/C$_\odot$ (number)	+0.81
log N/O − log N$_\odot$/O$_\odot$ (number)	+0.32

Notes. Although this mass-loss rate of 10^{-10} M$_\odot$ yr^{-1} appears to be a reasonable upper limit resulting from the CMFGEN model, in the text we discuss why a higher upper limit of 10^{-8} M$_\odot$ yr^{-1} is probably more important, due to a possible lack of cooling in the wind.

velocity law as input that is typically parametrized by a β-type law, which is modified to smoothly match a hydrostatic structure at high optical depths. The current version of CMFGEN iterates to fulfill the equation of continuity below the sonic point. Here we assume $\beta = 1.5$. We do not include the effects of clumping. We refer the reader to these aforementioned papers and Hillier & Miller (1998) for further details on CMFGEN.

We employed standard spectroscopic criteria (see e.g. Crowther, Lennon & Walborn 2006; Searle et al. 2008) for determining the stellar and wind parameters of SBW1. These criteria are further detailed below. In summary, we first estimated the effective temperature using the Si ionization balance and the effective gravity using the wings of Hγ, Hβ and Hα. We then estimated the microtubulent velocity (10 km s^{-1}) based on the strength of the Si III λλλ4552, 4668, 4575 lines. We readjusted $T_{\rm eff}$ and log $g_{\rm eff}$ to still fit the spectrum. The abundances were then determined by producing models with different abundances of a given element until the best fit was achieved. The luminosity of the best-fitting model and the reddening parameters were then adjusted to fit the observed UV, optical and IR flux. Table 2 presents the inferred stellar and wind parameters, while Figs 1 and 2 show the best-fitting CMFGEN model compared to the observations of SBW1 in the optical and UV, respectively.

We find log $g_{\rm eff} = 3.0 \pm 0.1$ based on the wings of Hγ, Hβ and Hα in the high-resolution spectra of SBW 1. Our models indicate $T_{\rm eff} = 21\,000 \pm 1000$ K based on the ionization balance of Si, using the relative strengths of Si IV λ4088, Si III λλλ4552, 4668, 4575 and Si II λ4128. The value of the effective temperature is further supported by the He and Fe ionization balances, using He II λ1640 in the UV and optical He I line triplets (since singlets are model-dependent; Najarro et al. 2006), and UV Fe III and Fe IV lines.

The luminosity of SBW1 is more difficult to constrain because the distance and reddening are uncertain. With the CMFGEN model, we can constrain the reddening using the observed optical to near-IR magnitudes (Smith et al. 2007, 2013), and the flux-calibrated COS spectrum in the UV, combined with an assumed distance. We compared the observed spectral energy distribution (SED) with CMFGEN models computed with different luminosities, and reddened using the parametrization from Fitzpatrick (1999), but with a variety of values of R_V. The distance to SBW1 is uncertain, derived previously from its radial velocity as ∼7 kpc (Smith et al. 2007). We find a bolometric luminosity of $L_\star = 5.5(\pm1.0) \times 10^4$ L$_\odot$ (D/7 kpc)^2 and a colour excess of $E(B-V) = 1.08$ mag, assuming a selective-to-total extinction parameter of $R_V = 3.8$.

Fig. 3 shows the observed COS spectrum in the UV and the optical/IR photometry compared to a model SED with these parameters. While the UV, *R* and near-IR are well fitted, the *V*-band photometry appears to be discrepant. We suspect that this *V*-band mismatch is due to a large uncertainty in the *V* magnitude; as noted by Smith et al. (2007), this *V*-band magnitude of 12.7 comes from the GSC 2.2 catalogue, which is based on an estimate of the magnitude in photographic plate data, and approximated to the *V* band. Such magnitude estimates from photographic plate data may be compromised by the presence of a dusty nebula around SBW1 (Smith et al. 2013), so we regard this *V*-band magnitude as questionable (certainly less reliable than the *JHK* photometry from 2MASS). In any case, modern photometry of SBW1 would be useful. The value of $R_V = 3.8$ instead of 3.1 is not so surprising, since there may be anomalous extinction from a multicomponent and peculiar line of sight (through the Carina Nebula H II region, plus cold interstellar medium along the line of sight) and/or extinction due to the circumstellar nebula. Indeed, a value of $R_{\rm V} = 4.8$ has been determined for local clouds within the Carina Nebula (Smith 2002), through which SBW1 is seen. Combining this with $R_V = 3.1$ for other portions of the same line of sight might yield an intermediate value for the total. Thus, we find a best fit for $E(B-V) = 1.08$ mag and $R_V = 3.8$. For these, we find a 5.5×10^4 L$_\odot$ for an assumed distance of 7 kpc, as noted above. Since the uncertainty here is dominated by our choice to de-weight the *V* band, we adopt an error bar in the luminosity of about 20 per cent (for an assumed distance), or $\pm\ 1 \times 10^4$ L$_\odot$. The distance, luminosity and mass of the star are discussed further in Section 4.1.

Using the relative strength of optical He I to H lines, our CMFGEN analysis indicates that the He abundance of SBW1 is around solar, with He/H = 0.1 (by number). We use C II λ4267 as a diagnostic for the C abundance, O II λλ4070, 4317, 4367, 4596, 4650, 4661 for O, and N II λλ3995, 4447, 4630 for N. We find 12 + log C/H = 7.84, 12 + log N/H = 8.13 and 12 + log O/H = 8.30, implying that N is enriched in comparison to C and O. The abundances of SBW1 are within the range of typical values inferred for BSGs by Crowther et al. (2006) and Searle et al. (2008).

Remarkably, the observed spectrum of SBW1 does not show any clear signature of wind emission in the UV and optical regions, which suggests a very low value of $\dot{M}$. We computed CMFGEN models with $\dot{M}$ values between 10^{-10} and 10^{-5} M$_\odot$ yr^{-1}. While Hα is contaminated by nebular emission, significant emission would still be detectable for $\dot{M} \gtrsim 10^{-6}$ M$_\odot$ yr^{-1}, and wind signatures could possibly be detected down to $\dot{M} \gtrsim 10^{-7}$ M$_\odot$ yr^{-1}. The UV resonance lines provide more stringent constraints on $\dot{M}$. Even a model with 10^{-10} M$_\odot$ yr^{-1} still shows significant Si IV λλ1394,1402 emission, which is not detected in the observed spectrum (upper panel of Fig. 2). Interestingly, a CMFGEN plane–parallel model (i.e. no wind, just photospheric emission) provides a better match to the observed UV spectrum of the S IV lines (see Fig. 2). As such, CMFGEN models suggest that the mass-loss rate of SBW1 is less than 10^{-10} M$_\odot$ yr^{-1}. Any possible optically thin wind clumping (which we have not included) would lower this estimate even more. (Note that this plane-parallel model and the low-mass-loss-rate wind model have no detectable difference in the near-IR due to free–free

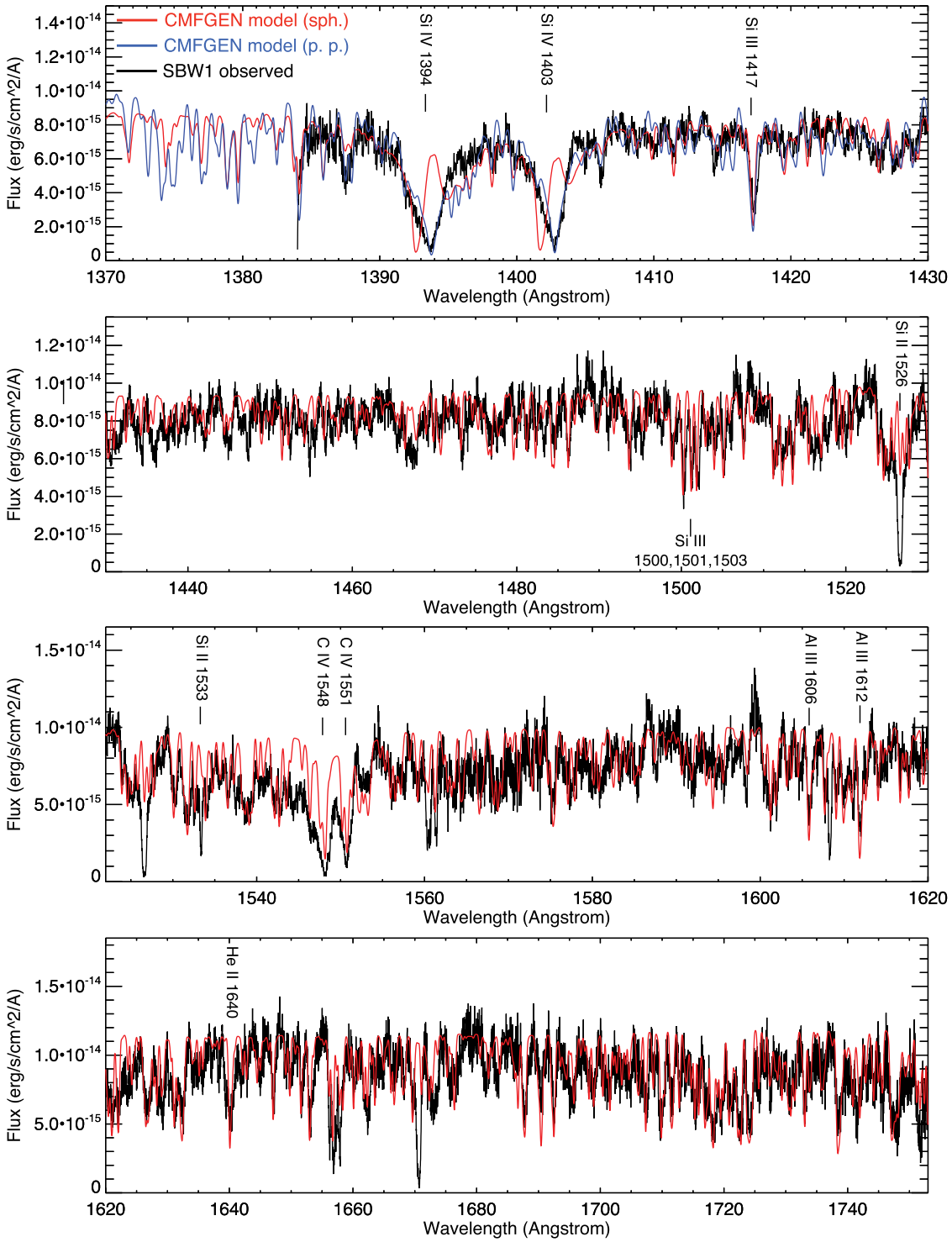

Figure 2. Similar to Fig. 1, but in the UV region between 1370 and 1750 Å. The strongest spectral lines are identified, while the remaining features are mostly due to Fe III, Fe IV or Ni III lines. This figure also includes a plane–parallel CMFGEN model in the UV (top panel, in blue) to illustrate the atmospheric spectrum with no wind.

wind emission.) As we discuss below, however, there are reasons to suspect that some of the approximations in CMFGEN may no longer be appropriate much below $10^{-8}\,M_{\odot}\,yr^{-1}$, due to the balance of heating and cooling (and its influence on the ionization level). We therefore adopt this latter value as a conservative upper limit in our analysis. Because wind signatures are not detected, we cannot place constraints on the wind terminal velocity of SBW1's wind. The models analysed here assume $v_{\infty} = 300\,km\,s^{-1}$ and $\beta = 1.0$.

To further investigate the low value of $\dot{M}$ for SBW1, we inspected publicly available *IUE* UV spectra of BSGs. Fig. 4 compares the

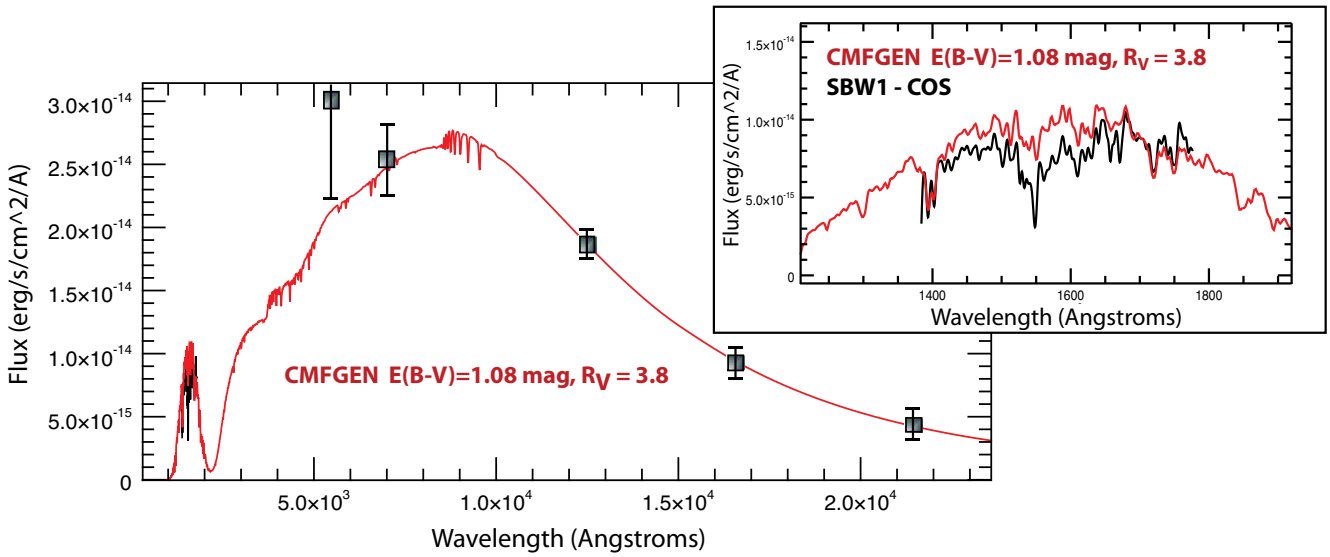

Figure 3. UV to near-IR spectral energy distribution (SED) of SBW1, including the observed COS spectrum (black) and the CMFGEN model (red) with the best-fitting extinction parameters of $E(B-V) = 1.08$ mag and $R_V = 3.8$. The photometry is from Smith et al. (2013); we have enlarged the error bars on the V and R bands, since these are from the GSC 2.2 catalogue, with magnitudes estimated from photographic plates where the presence of the nebula may influence the apparent brightness. The inset at top right-hand side is a zoom-on on only the UV, but with the same parameters. The observed COS spectrum and the model have been smoothed to lower resolution for clarity.

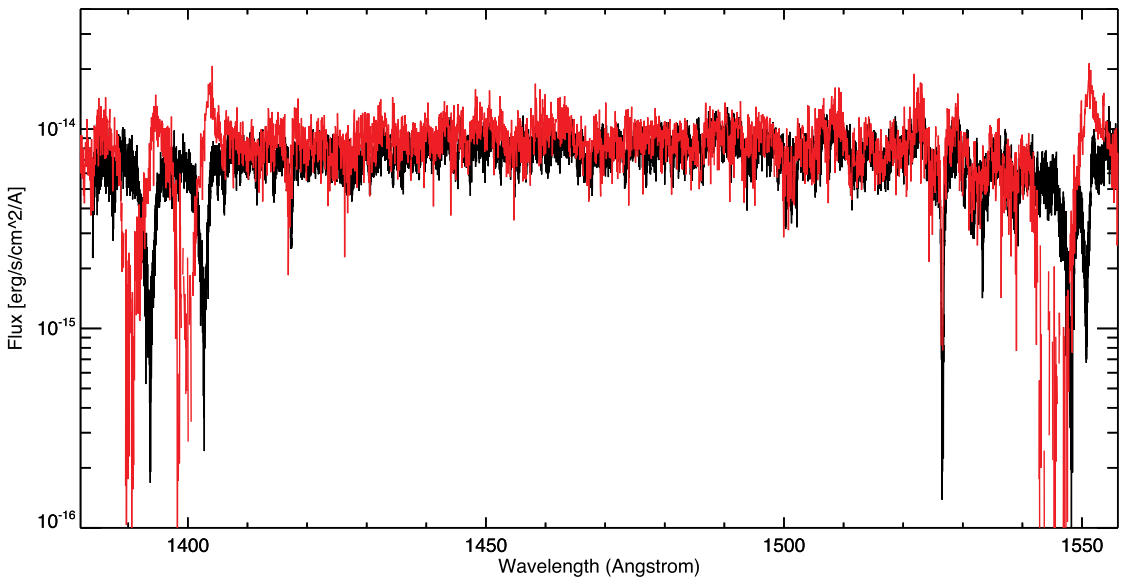

Figure 4. Comparison between the UV spectrum of SBW 1 (B1.5 Iab; black) and HD 13854 (B1 Iab; red). HD 13854 was scaled to roughly match the continuum flux of SBW1. Note the stronger Si IV and C IV resonance lines in the latter because of the higher mass-loss rate.

UV spectrum of SBW1 to that of HD 13854, which is a B1 Iab supergiant star (Searle et al. 2008). One can clearly see that despite having a very similar photospheric spectrum, the Si IV and C IV lines have P Cyg profiles and are much stronger in HD 13854, indicating a significantly stronger wind than in SBW1. Indeed, Searle et al. (2008) estimated a mass-loss rate of 1.5×10^{-6} $M_\odot$ yr^{-1} for HD 13854, which is several orders of magnitude larger than for SBW1, and consistent with expectations. This difference may be related to the significantly different luminosities of these two BSGs (3.4×10^5 $L_\odot$ for HD 13854), which would cause different mass-loss rates due to the difference in radiative flux. Even so, it is puzzling that SBW1's wind is so weak.

4 DISCUSSION

4.1 Central star properties

Our CMFGEN analysis confirms many of the physical paramaters that had been inferred previously from photometry and spectral type. The value of $T_{\rm eff} = 21\,000$ K that we derive from the CMFGEN model is the same as assumed previously from the B1.5 Iab spectral type and SED (Smith et al. 2007, 2013). The luminosity derived previously from the SED was uncertain $(0.5–1) \times 10^5$ $L_\odot$ (Smith et al. 2013). Our CMFGEN model gives a consistent but perhaps somewhat lower value of 5.5×10^4 $L_\odot$ D_7^2, where D_7 is the distance relative to our assumed value of 7 kpc.

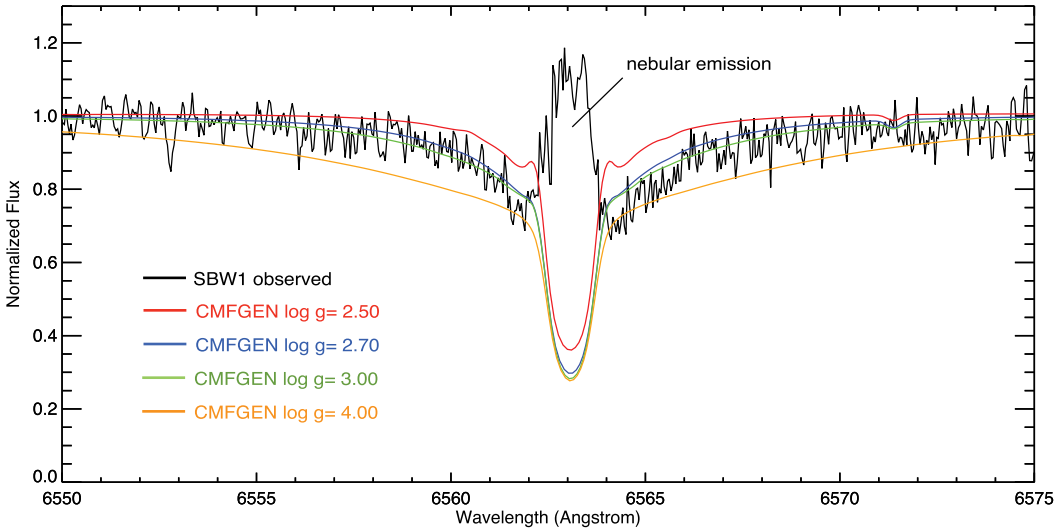

Figure 5. Detail of the Hα line profile in an echelle spectrum of the star obtained with EMMI (from Smith et al. 2007). The emission at line centre is due to nebular emission from the ring (this is clear in resolved long-slit spectra; see Smith et al. 2007), but the line wings trace the photospheric absorption profile due to pressure broadening. The rotation rate is only $\sim$40 km s^{-1} (Taylor et al. 2014), so rotation does not alter the broad-line wings. To this high-resolution spectrum, we compare CMFGEN models with the same parameters as discussed above, except that we explore different values of the effective gravity. From this comparison, it is evident that log $g_{\rm eff} = 2.5$ (cgs units) is too low and 4.0 is too high, but log $g_{\rm eff}$ values of 2.7–3.0 provide a good match to the data, with 3.0 being somewhat preferred in some wavelength ranges.

Interestingly, with the weak wind of SBW1, we can use the effective gravity $g_{\rm eff}$ from the model to place constraints on both the true luminosity and present-day mass if we assume that the spectroscopically derived mass $M_{\rm spec}$ is comparable to the evolutionary mass $M_{\rm evo}$. Langer & Kudritzki (2014) have discussed this in detail, and concluded that $M_{\rm spec}$ is usually a reliable representation of the true stellar mass as long as the star is not close to the Eddington limit (i.e. for moderately massive and intermediate-mass stars). Since SBW1 has no detectable signatures of a wind, we surmise that it is nowhere near its Eddington limit. Comparing CMFGEN models to high-resolution echelle spectra of Balmer lines, as shown in Figs 1 and 5, we favour a value of 3.0 for log $g_{\rm eff}$. From the definition of $g_{\rm eff} = GM/R^2$, we can write

$$M_{\rm spec} = \frac{g_{\rm eff}\, R_*^2}{G} = \frac{g_{\rm eff}\, L_*}{4\pi\sigma\, G\, T_{\rm eff}^4},$$

where $M_{\rm spec}$ is the present-day spectroscopically derived stellar mass, R_* and L_* are the star's photospheric radius and bolometric luminosity, respectively, σ is the Stefan–Boltzmann constant and G is the gravitational constant. Inserting fiducial values of $T_{\rm eff}$ = 21 000 K, $g_3 = (g_{\rm eff}/10^3 {\rm cm\,s^{-2}})$ and $L_* = 5.5 \times 10^4 L_\odot\ (D_7)^2$, where D_7 is the adopted distance relative to 7 kpc, we then have

$$M_{\rm spec} \approx 15\ {\rm M}_\odot\ (g_3\, D_7^2)$$

for the *present-day* stellar mass as indicated by the effective gravity. We can then attempt to constrain the actual luminosity and mass of SBW1 by seeing what combinations of D, L_*, $g_{\rm eff}$ and $M_{\rm spec}$ give values consistent with evolutionary models. Fig. 6 shows a Hertzsprung–Russel (HR) diagram comparing the inferred luminosity of SBW1 to single-star evolutionary tracks (Brott et al. 2011), for reference. This comparison shows that the luminosity for an assumed distance of 7 kpc, combined with the $g_{\rm eff}$ indicated by the spectrum, gives a stellar mass of $\sim$15 M$_\odot$ – and this is in very good agreement with what one expects for the position in the HR diagram compared to single-star models. For an even smaller distance around 4 kpc, this discrepancy gets much worse (see Fig. 6). For a slightly larger distance of 9.9 kpc, the luminosity and $M_{\rm spec}$ rise by a factor of two, and importantly, are then underluminous/overmassive compared to models in that part of the HR diagram. For $D = 7$ kpc, however, the $T_{\rm eff}$ and L_* we derive would agree very well with the hook in the evolutionary track for a 15 M$_\odot$ star that occurs after core H exhaustion, which would seem to make sense with the BSG spectral type. Of course, the comparison to single-star evolutionary tracks may be misleading if SBW1 is the result of binary evolution that may alter its L/M ratio; one could argue that it would be appropriate to compare SBW1's spectroscopic mass to models for a merger product or mass gainer. Such a comparison might favour a slightly different combination of D, $g_{\rm eff}$, L_* and M_*, especially if these values evolve in the $\sim 10^4$ yr after a merger or mass transfer episode. Nevertheless, this comparison with single-star models makes a case that the adopted distance, reddening – and consequently, luminosity and mass – are reasonable values.

The luminosity is unlikely to be much lower than 3×10^4 L$_\odot$, however, due to the fact that the optical spectrum has a supergiant luminosity class. Note that line ratios such as Si III λ4552/He I λ4387 are the primary criteria for luminosity class in this temperature range, not widths of Balmer lines (Walborn 1971). Also, the implied mass from $g_{\rm eff}$ would be too low for the corresponding L if the distance were closer. At 4 kpc, for example, we would have log(L/L$_\odot$) = 4.2. However, at this L, $g_{\rm eff} = 3$ would imply a stellar mass of only $\sim$5 M$_\odot$ (see Fig. 6), but a star of that mass will never get so luminous. Based on this comparison, we therefore favour values of log $g_{\rm eff} = 3.0$ cm s^{-2} and $L_* = 5.5 \times 10^4$ L$_\odot$ for SBW1.

Altogether, these parameters make the central star of SBW1 only a little hotter than Sk−69°202, and about 50 per cent of its bolometric luminosity. It has an effective initial mass of around 15 M$_\odot$, as compared to 18 M$_\odot$ for Sk−69°202 (Arnett 1989; Arnett et al. 1989). From $L \propto R^2 T_{\rm eff}^4$, the implied stellar radius is roughly 15–20 R$_\odot$, and so the surface escape velocity is about the same as for the Sun or slightly lower.

The chemical abundances we derive from the photospheric spectrum show basically Solar composition, except for an enhanced N

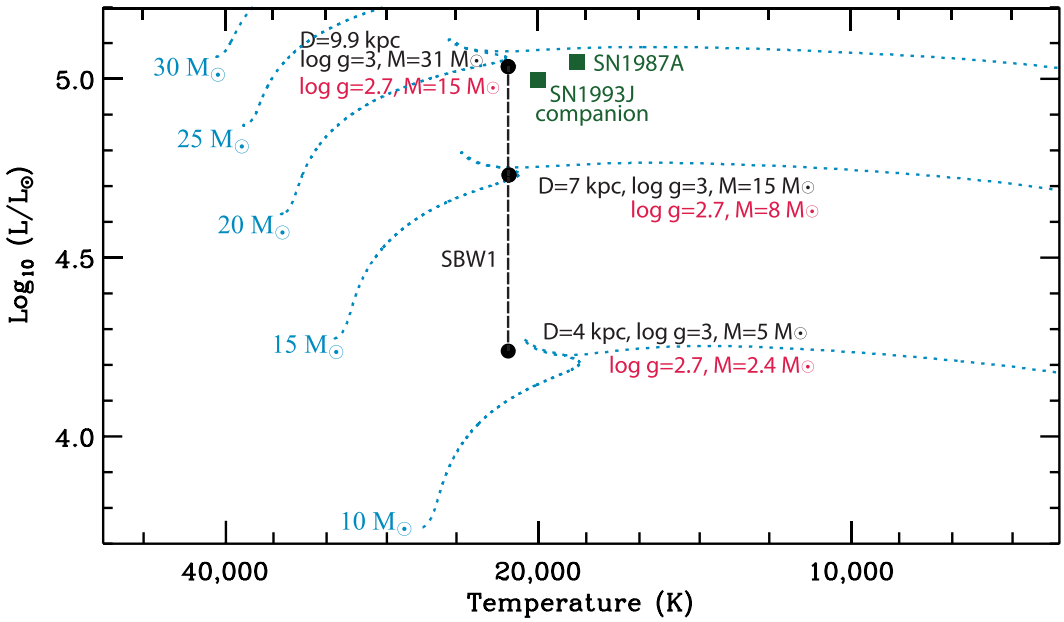

Figure 6. HR diagram with representative single-star evolution tracks from Brott et al. (2011). We denote the location of the progenitor stars of SN 1987A (Maund et al. 2004) and the companion of SN 1993J (Fox et al. 2014), as compared to SBW1. For SBW1, the three black filled dots show the luminosity indicated by our CMFGEN model for assumed distances of $D_7 = 7$ kpc, $\sqrt{2} \times D_7 = 9.9$ and 4 kpc, while the red and black text give the implied present-day stellar masses for log $g_{\rm eff} = 2.7$ and 3, respectively. The implication is that an assumed distance of 7 kpc is actually pretty good, because $g_{\rm eff}$ gives stellar masses that are in good agreement with the mass one would infer from comparing the luminosity to evolutionary tracks. A distance of 4 kpc is far too small. A slightly larger distance of 9.9 kpc gives double the luminosity and stellar mass, and is also in poor agreement with the luminosity for evolutionary models if we adopt log $g_{\rm eff} = 3$.

abundance that is elevated by a factor of 2–6 compared to solar N/O or N/C ratios, respectively. This too is quite similar to the enhanced N abundances inferred from the emission-line spectrum of the ring around SN 1987A, and is indicative of significant CNO processing present at the star's surface.

Will the central star of SBW1 be the next Galactic SN? The dynamical age of the nebula is about 10^4 yr, similar to SN 1987A, so perhaps it is a good candidate. Of course, the uncertainty of such a clock is huge. Aside from the nebular age and an analogy to SN 1987A, we have little from which to infer the time until the impending core collapse.

4.2 Stellar wind properties

The most significant observational result from our COS spectrum is the lack of any strong wind features in the spectrum, which is very unusual for a BSG. Consequently, the most interesting result from our quantitative CMFGEN analysis is the astonishingly low derived mass-loss rate of SBW1. Comparing our lowest mass-loss rate CMFGEN models (which still show some evidence of wind emission) to the observations, which show none, implies and upper limit of $\dot{M} < 10^{-10}$ M$_\odot$ yr^{-1} for an assumed terminal wind speed of 300 km s^{-1}. However, this assumes that the UV resonance lines are modelled correctly at such low wind densities.

A cautionary remark relates to the so-called 'weak-wind problem' (see Smith 2014 for a review), where UV diagnostics of late-type O dwarfs yield mass-loss rates that are 100 times lower than expected from the Vink et al. recipe and from Hα diagnostics. The cautionary comment is that an independent method of deriving the mass-loss rate based on the structure of a bow shock around ζ Oph gives a mass-loss rate estimate that is ∼10 times higher than UV diagnostics, but still an order of magnitude lower than expected from standard mass-loss prescriptions (Gvaramadze, Langer & Mackey 2012). Thus, there are some indications that the weak-wind problem for late O dwarfs is perhaps not as severe as indicated by UV estimates. Thus, when mass-loss rates are low, CMFGEN and similar models might underestimate the mass-loss rate somewhat based on UV diagnostics. This may be caused by inefficient cooling at low wind densities, so that shocks within the wind keep the ionization level higher than expected (Bouret et al. 2015; Puebla et al. 2016). Does some version of this weak wind problem translate to BSG winds such as the case of SBW1?

Fig. 7 shows how the flow time-scale in the wind compares to the cooling time-scale for some representative assumed values of the mass-loss rate and the collision speed U_0 of internal shocks in the wind. The temperature and ionization balance of the wind depends on heating by shocks within the flow, and cooling, which depends on the density. If the cooling time-scale becomes long at low densities, the wind may expand before it can cool, and so the ionization in the inner wind may be higher than in a CMFGEN model. Typical wind speeds for an early B supergiant would be around 500 km s^{-1}, and we would expect shocks within the clumpy outflowing wind to be some fraction of that – perhaps 100–200 km s^{-1} – and almost certainly less than 300 km s^{-1} (a caveat is that we cannot be certain about the value of the wind speed, since we do not actually detect any wind absorption; thus, it remains possible that SBW1's wind might be faster than typical winds for B1.5 supergiants, which might raise the allowed mass-loss rate). Therefore, in Fig. 7, we should expect SBW1's wind to reside somewhere above the green dashed line and below the blue dash–dotted line (for $U_0 = 100$ and 300 km s^{-1}, respectively). For an intermediate shock speed around 200 km s^{-1}, for example, a mass-loss rate below 10^{-8} M$_\odot$ yr^{-1} would make the cooling time-scale and the flow time-scale about the same in the inner wind (a few stellar radii). This means that below

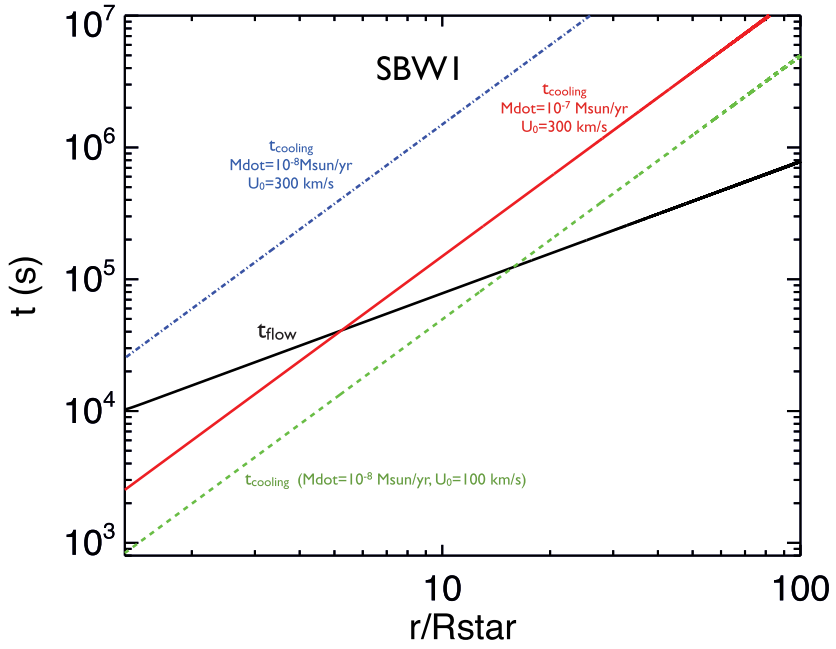

Figure 7. Plot of the flow time-scale (black solid line) compared to the cooling time-scale in a CMFGEN model as a function of radius for some representative assumed values of mass-loss rate and shock velocity U_0. If the wind outflow speed is 300–500 km s^{-1}, then the typical speed of internal shocks in the wind is probably 100–200 km^{-1} or less, and very likely less than 300 km s^{-1}. Thus, we see that for expected shock speeds, the wind cooling time-scale becomes comparable to the flow time-scale in the inner wind when the mass-loss rate drops below 10^{-8} M$_\odot$ yr^{-1}. As such, it is possible that UV diagnostics become less reliable at such low wind densities due to increased ionization.

10^{-8} M$_\odot$ yr^{-1}, the bulk of the wind might remain hotter than in the CMFGEN model, and would be harder to observe in the typical UV diagnostic lines that we are referring to. Thus, if the mass-loss rate drops much below 10^{-8} M$_\odot$ yr^{-1}, we cannot be confident that CMFGEN is properly treating the relevant physics, whereas above this, we should begin to see some evidence of a wind in the UV lines. We adopt 10^{-8} M$_\odot$ yr^{-1} as a fairly conservative upper limit to the mass-loss rate of SBW1, rather than 10^{-10} M$_\odot$ yr^{-1}, due to this uncertain treatment of the cooling and ionization balance in CMFGEN at such low mass-loss rates.

Our hypothesis that the wind of SBW1 has too low a density to cool – and therefore remains hot – can be tested. This hypothesis would predict detectable X-ray, extreme-UV and possibly FUV emission signatures from the wind, which may be verified with future observations. An observational determination of $L_X/L_{\rm Bol}$ with future X-ray observations would thus help provide a direct constraint on the mass-loss rate of SBW1 and the amount of shock heating within the wind. At the stellar temperatures appropriate for SBW1's spectral type, CMFGEN does not predict any N V or O VI features, but CMFGEN's treatment of the wind is not appropriate if the wind remains hot as we suspect. If low density inhibits cooling, we can make a qualitative prediction that N V and O VI may be observed (see e.g. Zsargo et al. 2008; Bouret et al. 2015; Puebla et al. 2016), but a more detailed model beyond CMFGEN's current capabilities would be needed to derive a specific line strength for a quantitative mass-loss rate.

Even this revised upper limit to the mass-loss rate of 10^{-8} is much lower than one would expect for this star. For example, from the mass-loss prescriptions given by Vink, de Koter & Lamers (2001), we would expect $\dot{M} = 1.2\times 10^{-7}$ M$_\odot$ yr^{-1} for $L = 5 \times 10^4$ L$_\odot$, for line-driven winds at the appropriate $T_{\rm eff}$ of SBW1 (note that 21 000 K places this on the cool side of the bistability jump). Our observationally derived upper limit to the mass-loss rate for SBW1 is more than 10 times lower than this expected value, even with no reduction in the observed value to correct for clumping.

Why is the wind of SBW1 so weak as compared to expectations, and as compared to other observed BSGs? The solution to this puzzle may hold important clues related to the origin of the ring nebula and the star's evolutionary history, and perhaps also for extragalactic SNe that appear similar to SN 1987A.

For SN 1987A, the physical properties of the pre-SN stellar wind were uncertain, but some considerations also pointed to an anomalously low mass-loss rate compared to other BSGs. On the one hand, models derived from interpreting the early radio observations in the context of free–free self-absorption of the SN radio emission by the freely expanding wind yielded a relatively high mass-loss rate of the order of (3.5–6) $\times$ 10^{-6} M$_\odot$ yr^{-1} with $v_{\rm w} = 550$ km s^{-1} (Chevalier & Fransson 1987; Lundqvist & Fransson 1991; Chevalier & Dwarkadas 1995). On the other hand, hydrodynamic interacting-winds models used to explain the formation of the nebula required much weaker BSG winds in order to reproduce the slow expansion speed of the equatorial ring (Blondin & Lundqvist 1993; Martin & Arnett 1995). To keep the ring expanding at the slow observed value of $\sim$10 km s^{-1}, these models would require upper limits to the mass-loss rate and wind speed of $\dot{M} < 3 \times 10^{-7}$ M$_\odot$ yr^{-1} and $v_{\rm w} < 300$ km s^{-1}. Blondin & Lundqvist (1993) suggested that this discrepancy might be explained if the star's mass-loss rate increased in the last decades or century leading up to the moment of explosion, but Chevalier & Dwarkadas (1995) suggested that synchrotron self-absorption, rather than free–free self-absorption by the wind, might explain the early radio observations.

Further indication that the progenitor star's mass-loss rate was low compared to normal BSGs came from the rebrightening in the radio at $\sim$1500 d after the SN (Staveley-Smith et al. 1992, 1993; Gaensler et al. 1997, 2000; Manchester et al. 2002; Zanardo et al. 2013). This rebrightening was attributed to the collision

between the fast SN ejecta and an H II region from the photoionized RSG wind, as noted in the Introduction (Chevalier & Dwarkadas 1995). Assuming that the interior region was filled with a relatively low-density freely expanding BSG wind, Chevalier & Dwarkadas (1995) showed that this collision could occur at the observationally inferred radius of ∼0.1 pc with a model that adopted $\dot{M} = 7.5 \times 10^{-8}$ $M_\odot$ yr^{-1} and $v_w = 450$ km s^{-1}. Later models refined this value, in some cases including constraints from the evolution of X-ray emission, to even lower values of around 5×10^{-9} $M_\odot$ yr^{-1} or less (Dwarkadas 2007; Dewey et al. 2012).

This is a very low mass-loss rate for a BSG star of $\sim 10^5$ $L_\odot$. According to the standard recipe for hot star mass-loss rates usually used in evolutionary codes (Vink et al. 2001), a star with $\log(L/L_\odot) = 5$, $T_{\rm eff} = 21\,000$ K, and $M = 18$ $M_\odot$ should have a mass-loss rate of 4.8×10^{-7} $M_\odot$ yr^{-1} at Large Magellanic Cloud (LMC) metallicity. The mass-loss rate inferred for the progenitor of SN 1987A based on the expansion of the blast wave is at least 6 and as much as 100 times lower than this expected value. This appears very similar to the case of SBW1 outlined above.

Thus, both the progenitors of SN 1987A and SBW1 seem to share the peculiarity that they have BSG winds that are extremely weak compared to the expected wind strength for their stellar parameters. This is not the case for the other two well-studied Galactic analogues with ring nebulae; both Sher 25 and HD 168625 have strong Hα wind emission and have mass-loss rates that are normal (Sher 25) or strong (HD 168625) compared to other BSGs (Nota et al. 1996; Smartt et al. 2002). Although accounting for clumping has been argued to require a reduction to mass-loss rate recipes by factors of 3–5 (see Smith 2014 for a review), the deficits for SN 1987A and SBW1 are greater than this (and again, we did not include a clumping correction for SBW1). The discrepancy might be ameliorated somewhat for SBW1 if it is at a nearer distance, despite clues noted above, but the distance to the LMC is more firmly established and would not resolve the same problem for SN 1987A.

In models that aim to explain the formation of SN 1987A's triple ring nebula with a merger (Morris & Podsiadlowski 2007, 2009), BSG mass-loss rates of (1–2) $\times 10^{-7}$ $M_\odot$ yr^{-1} are adopted to shape the ring nebula (e.g. table 4 in Morris & Podsiadlowski 2009). Recently, Orlando et al. (2015) adopted this same value for the mass-loss rate in their simulations of the SN interaction with the circumstellar material (CSM), although they did not explore the impact of other assumed values for the mass-loss rate. These are higher than the observationally inferred values for SN 1987A (from the time history of radio emission, as noted above) and for SBW1. It is therefore unclear if interacting stellar winds can provide a viable physical explanation for the shaping of the nebulae around SN 1987A and SBW1. The issue of pressure balance is discussed more below.

4.3 Implications for the nebula and the pre-SN evolution of SN 1987A

Previous studies have discussed the formation of bipolar and ring nebulae, like the ones around SN 1987A and SBW1, in the context of interacting winds where a fast BSG wind expands into a slower and asymmetric RSG wind with an equatorial density enhancement (see the Introduction). However, a somewhat different scenario was discussed wherein a fast BSG interacts with an H II region or photoevaporative flow for the specific cases of SN 1987A (Chevalier & Dwarkadas 1995) and SBW1 (Smith et al. 2013) based on the inferred density structure inside the ring, which is inconsistent with a simple interacting winds scenario. In this section, we discuss how the extreme weakness of the BSG wind from SBW1 requires further modification to the story.

In this scenario, the location of the shock between the BSG wind and the ionized photoevaporative flow is determined by the mass-loss rate and speed of the wind from the central star, balanced by the pressure of the photoevaporative flow. Specifically, ram pressure of the stellar wind $\rho\, v^2$ is balanced by the thermal pressure of the ionized gas inside the ring nebula. The photoevaporation rate of the ring, which is the source of gas and dust in the H II region, depends on geometry and the ionizing photon flux of the star, $Q_{\rm H}$, which is given in Table 1. However, in this case, we can avoid the uncertainty introduced by the detailed geometry of the ring (clump size, ring height, whether gas in the walls of an hourglass contributes, etc.) because spectral observations of the nebula (the Hα emission measure and the [S II] $\lambda\lambda$6717, 6731 line intensity ratio in the spatially resolved diffuse interior of the ring) directly constrain the density of the ionized flow filling the inside the ring to be roughly 300–500 cm^{-3} (Smith et al. 2013). (Note that the density inferred from the [S II] line ratio is independent of distance.) Thus, the ionized gas pressure is directly constrained observationally, and so the pressure there is known regardless of the geometry that creates it. While the pressure within this H II region is roughly uniform, the ram pressure of the wind drops with radius from the star if we assume a steady BSG wind (R^{-2} density profile). Then R is the radius where the two balance, given by

$$R \;=\; 0.05 \left(\dot{M}_{-7}\, V_{300} \right)^{1/2} \left(\frac{n_{\rm e}}{500\ {\rm cm}^{-3}} \right)^{-1/2} {\rm pc},$$

where we have assumed $T = 10^4$ K in the H II region, $\dot{M}_{-7}$ is the BSG wind mass-loss rate in units of 10^{-7} $M_\odot$ yr^{-1} and V_{300} is the wind speed in units of 300 km s^{-1}. We assumed a value for $V_{\rm BSG}$ of 300 km s^{-1}, as above. These fiducial values are similar to the values adopted for the progenitor of SN 1987A by Chevalier & Dwarkadas (1995).

With these values, the stand-off shock will be at $R \approx 0.05$ pc from the BSG. This is about 25 per cent of the radius of the ring (note that both SN 1987A and SBW1 have the same ring radius of ∼0.2 pc). In the case of SBW1, 25 per cent of the ring radius roughly matches the location of the observed inner peaks of hot dust and enhanced Hα emission in images, which is why we chose these fiducial values. Since the innermost dust near the shock front will be the hottest and brightest because it is radiatively heated by the star, we argued (Smith et al. 2013) that this physical scenario may give a plausible explanation for the structures inside the ring. We subsequently proposed to obtain UV spectra to directly constrain SBW1's mass-loss rate in order to test this picture.

We were therefore surprised to find a mass-loss rate for SBW1 that is at least an order of magnitude lower than the fiducial value above. With $\dot{M} < 10^{-8}$ $M_\odot$ yr^{-1} (a conservative upper limit), the radius of the stand-off shock between the BSG wind and the ionized photoevaporative flow should be much smaller, roughly <0.015 pc or only about 5–10 per cent of the ring's radius. Essentially, the BSG wind is so weak that it would be overwhelmed by the gas pressure of the photoionized photoevaporative flow. Colliding winds may therefore have difficulty explaining the pile-up of dust at the location of the observed IR peaks in images (Smith et al. 2013). A renewed investigation of this problem using hydrodynamic simulations is warranted.

What then causes the peaks of dust emission at ∼25 per cent of the radius of the ring (at $R \approx 0.05$ pc from the star)? As noted in our

previous paper (Smith et al. 2013), the observed dust temperature estimated from the SED is only about 190 K (and the expected equilibrium temperature is even lower at that radius) so 0.05 pc cannot mark the dust vaporization radius. Something else must hold back the dust and prevent it from flowing closer to the star. A possibility is that direct stellar radiation pressure on dust grains helps keep them at bay, and that collisions couple this radiation pressure on dust to the gas. Indeed, the magnitude of the radiation pressure $L/(4\pi R^2 c)$ inside the ring, for our derived stellar parameters of SBW1, is comparable to or greater than the inferred ionized gas pressure for $T = 10^4$ K and $n_e = 500$ cm^{-3}, suggesting that direct radiation pressure on dust should affect the structure and dynamics of the interior of the ring.

So far, radiation pressure has not been included in simulations aiming to explain the origin and shaping of BSG rings like the ones around SN 1987A and SBW1. However, the weakness of the observed wind from SBW1 reported here (as well as the inferred weakness of the wind of SN 1987A's progenitor) suggest that this should be undertaken. Examining the hydrodynamics including radiation pressure is beyond the scope of this paper, but we note that the problem is reminiscent of recent studies of the dynamics and structure of dusty H II regions, where radiation pressure on dust is also found to be important (Krumholz & Matzner 2009; Draine 2011; Kim, Kim & Ostriker 2016). The relative influence of radiation pressure is even stronger in the case of SBW1 due to its extremely weak stellar wind for its luminosity.

Another possibility, which is difficult to rule out, is that the inner dust peaks arise from a past eruptive mass ejection akin to LBV eruptions (Smith et al. 2011a). While the BSG wind cannot form dust in its steady wind, it could potentially form dust in an episodic ejection of a dense shell (see e.g. Kochanek 2011). This dust shell might then expand until it is stopped by the pressure of the photoevaporative flow, leaving a cavity in its wake to be filled by the very weak BSG wind. In this case, it would be the momentum of the (hypothetical) eruptive mass ejection rather than the ram pressure of the BSG wind that would set the location of the inner dust peaks. This scenario is admittedly somewhat *ad hoc* and hard to constrain, but there is a precedent for it. Sequential episodic ejections of rings have been inferred based on direct proper motions of the ring nebula around the massive binary RY Scuti (Smith et al. 2011b), for example. For a somewhat different type of system, hydrodynamic simulations of nova eruptions inside a slow, equatorially concentrated CSM produced by Roche-lobe overflow (RLOF) can yield a similar torus structure with inner density peaks (Booth, Mohamed & Podsiadlowski 2016).

4.4 Spin-down

The very weak wind of SBW1 has an important consequence regarding the star's rotational evolution (e.g. Meynet, Eggenberger & Maeder 2011). Such a low mass-loss rate will impair the star's ability to shed angular momentum via its wind. SBW1 currently has a rather slow rotation rate, with an equatorial rotation speed of only about 40 km s^{-1} (Taylor et al. 2014), which is only about 5 per cent of its critical rotation speed.

The current slow rotation rate coupled with the currently observed very low wind mass-loss rate presents a puzzle in connection with the observed ring nebula. As noted in the Introduction, most scenarios to explain the existence of ring nebulae like the ones around SN 1987A and SBW1 invoke either (1) mass transfer through RLOF in an interacting binary (which would spin-up the mass gainer and then shed mass through the outer Lagrange point), (2) the merger of a close binary system resulting in a rapid rotator that excretes a disc, ring, or torus in the merger, or (3) post-RSG contraction to a BSG, spinning the star up to a rapidly rotating star that sheds an equatorial disc. All of these include a star that is rotating at or close to critical rotation when the ring is ejected. In the case of SBW1, the ring is only about 10^4 yr old (Smith et al. 2007, 2013).

The puzzle then is how a star can go from (presumably) nearly critical rotation (several 10^2 km s^{-1}) to being such a slow rotator (only 40 km s^{-1}) in such a short time if its wind is very weak. In this time, the star would shed a tiny fraction ($\sim 10^{-5}$ or less) of its total mass.

Magnetic braking would be the key mechanism to spin-down the star, and indeed, it has been suggested that a stellar merger event – which might eject a ring – might also lead to very strong stellar magnetic fields (Schneider et al. 2016). However, one expects the loss of angular momentum via magnetic breaking to be directly proportional to the mass-loss rate, which, in the case of SBW1, is exceedingly low. Even for massive stars with very strong (a few to several kG) fields and stronger winds, the spin-down time-scale is a few to several Myr (ud Doula, Owocki & Townsend 2009), not 10^4 yr. Indeed, using a parametrized estimate for the spin-down time from equation (25) in ud Doula et al. (2009), and adopting a generous 3 kG magnetic field, the parameters we estimate for SBW1 would suggest a spin-down time-scale of >6 Myr. It is therefore difficult to understand how the star could have slowed its rotation rate during the age of the nebula of only 10^4 yr unless the mass-loss rate was much higher in the past.

Ways out of this puzzle may require some different ideas. Observationally, at least, the gas and dust that partly fills the interior of the ring (Smith et al. 2013) could be interpreted as evidence for a previous high $\dot{M}$ phase, with a slow, dense, dusty wind that followed a merger and the ring's ejection. Perhaps a highly time variable wind or eruption needs to be invoked to help resolve this issue. Alternatively, perhaps a merger scenario different from proposed models is in order. For example, a merger of two blue stars (rather than a RSG) may lead to an envelope that is out of thermal equilibrium, as rotational energy is used to heat the merger product's envelope. The subsequent inflation of that envelope might allow a merger product to have a slow surface rotation rate at such a young age after a merger event. It is difficult to see how very rapid rotation can be avoided in a scenario wherein a merger occurs as a RSG, and then the merger product contracts to the blue while also maintaining a very low mass-loss rate. The low BSG wind mass-loss rate that we derive here is therefore an important constraint for models that aim to explain the origin and shaping of such ring nebulae with a merger event.

SBW1 may be an interesting target for spectropolarimetry to investigate the possibility of a strong magnetic field, although this may be complicated by large interstellar polarization. It is interesting to note that some models predict that magnetic massive stars can avoid the RSG phase altogether, staying blue and exploding as BSGs (Petermann et al. 2015). How this BSG star can avoid driving a much stronger wind with its current luminosity remains puzzling.

5 SUMMARY

We obtained a UV spectrum of the BSG SBW1 using *HST*/COS, with the aim of measuring the star's mass-loss rate in order to test a hypothesis regarding the shaping of the ring nebula. A CMFGEN model was used to analyse this spectrum.

We were surprised to find that the UV spectrum showed no signatures of wind emission or absorption, and the CMFGEN model yielded a conservative upper limit to the mass-loss rate of 10^{-10} M$_\odot$ yr^{-1}. However, we suspect that the mass-loss rate of

SBW1 is low enough that the UV diagnostics modelled by CMFGEN are not good tracers of the wind, probably because the wind is unable to cool at such low density. We find that the cooling time-scale is similar to or longer than the flow time-scale in the inner wind if the mass-loss rate falls below 10^{-8} $M_{\odot}$ yr^{-1}, and adopt this value as a more likely upper limit for the wind mass-loss rate.

Even 10^{-8} $M_{\odot}$ yr^{-1} is much lower than expected for a BSG with SBW1's physical parameters. This may present a problem for shaping the ring nebula with stellar wind interaction alone. We therefore speculate that radiation pressure on dust entrained in the photoevaporative flow off the ring may play an important dynamic role in shaping the nebula. Moreover, the very weak wind will inhibit the star's ability to shed angular momentum, which is problematic given SBW1's slow observed rotation speed of $\sim$40 km s^{-1}. Even with a generous magnetic field, we find that the likely spin-down time-scale is several Myr, which is much longer than the $\sim 10^4$ yr age of the ring nebula. This makes it difficult to understand how the ring could have been ejected in a merger event, which would be expected to leave behind a rapidly rotating star.

Based on the time dependence of radio emission, SN 1987A was also inferred to have a very weak wind for its progenitor's physical parameters, so our finding for SBW1 may affect ideas about SN 1987A's pre-SN evolution and the shaping of its nebula.

ACKNOWLEDGEMENTS

We thank John Hillier for maintaining CMFGEN and for continuing to make it available to the community, and also for advice on interpreting the very low mass-loss rate implied by the model in this case. We also thank an anonymous referee for helpful suggestions. Support was provided by the National Aeronautics and Space Administration (NASA) through *HST* grants GO-12924, GO-11637, GO-11977, GO-13390 and GO-13791 from the Space Telescope Science Institute, which is operated by AURA, Inc., under NASA contract NAS5-26555. NS also received partial support from NSF grants AST-1210599 and AST-1515559. JHG was supported by an Ambizione Fellowship of the Swiss National Science Foundation.

REFERENCES

Arnett W. D., 1987, ApJ, 319, 136
Arnett W. D., 1989, ApJ, 343, 834
Arnett W. D., Bahcall J. N., Kirshner R. P., Woosley S. E., 1989, ARA&A, 27, 629
Blondin J. M., Lundqvist P., 1993, ApJ, 405, 337
Booth R. A., Mohamed S., Podsiadlowski P., 2016, MNRAS, 457, 822
Bouret J. C., Lanz T., Hillier D. J., Martins F., Marcolino W. L. F., Depagne E., 2015, MNRAS, 449, 1545
Brandner W., Chu Y. H., Eisenhauer F., Grebel E. K., Points S. D., 1997, ApJ, 489, L153
Brott I. et al., 2011, A&A, 530, A115
Burrows C. J. et al., 1995, ApJ, 452, 680
Chevalier R. A., Dwarkadas V., 1995, ApJ, 452, L45
Chevalier R. A., Fransson C., 1987, Nature, 328, 44
Chita S. M., Langer N., van Marle A. J., Garca-Segura G., Heger A., 2008, A&A, 488, L37
Collins T. J. B., Frank A., Bjorkman J., Livio M., 1999, ApJ, 512, 322
Crotts A. P. S., Heathcote S. R., 2000, ApJ, 528, 426
Crotts A. P. S., Kunkel W. E., Heathcote S. R., 1995, ApJ, 438, 724
Crowther P. A., Lennon D. J., Walborn N. R., 2006, A&A, 446, 279
Dewey D., Dwarkadas V. V., Haberl F., Sturm R., Canizares C. R., 2012, ApJ, 752, 103
Draine B. T., 2011, ApJ, 732, 100
Dwarkadas V. V., 2007, Rev Mex. Astron. Astrofis., 30, 49
ud Doula A., Owocki S. P., Townsend R. H. D., 2009, MNRAS, 392, 1022
Fitzpatrick E. L., 1999, PASP, 111, 63
Fox O. D. et al., 2014, ApJ, 790, 17
Fransson C. et al., 2015, ApJ, 806, L19
Gaensler B. M., Manchester R. N., Stavely-Smith L., Tzioumis A. K., Reynolds J. E., Kesteven M. J., 1997, ApJ, 479, 845
Gaensler B. M., Manchester R. N., Stavely-Smith L., Wheaton V., Tzioumis A. K., 2000, in Kastner J., Soker N., Rappaport S., eds, ASP Conf. Ser. Vol. 199, Asymmetrical Planetary Nebulae II: From Origins to Microstructures. Astron. Soc. Pac., San Francisco, p. 449
Gvaramadze V. V., Langer N., Mackey J., 2012, MNRAS, 427, L50
Gvaramadze V. V. et al., 2015, MNRAS, 454, 219
Hillier D. J., Miller D. L., 1998, ApJ, 496, 407
Kim J. G., Kim W. T., Ostriker E. C., 2016, ApJ, 819, 137
Kochanek C. S., 2011, ApJ, 741, 37
Krumholz M. R., Matzner C. D., 2009, ApJ, 703, 1352
Langer N., Kudritzki R. P., 2014, A&A, 564, A52
Lundqvist P., Fransson C., 1991, ApJ, 380, 575
Luo D., McCray R., 1991, ApJ, 379, 659
Manchester R., Gaensler B. M., Wheaton V. C., Staveley-Smith L., Tzioumis A. K., Bizunok N. S., Kesteven M. J., Reynolds J. E., 2002, Publ. Astron. Soc. Aust., 19, 207
Martin C. L., Arnett W. D., 1995, ApJ, 447, 378
Maund J. R., Smartt S. J., Kudritzki R. P., Podsiadlowski P., Gilmore G. F., 2004, Nature, 427, 129
Meaburn J., Bryce M., Holloway A. J., 1995, A&A, 229, L1
Meynet G., Eggenberger P., Maeder A., 2011, A&A, 525, L11
Morris T., Podsiadlowski P., 2007, Science, 315, 1103
Morris T., Podsiadlowski P., 2009, MNRAS, 399, 515
Najarro F., Hillier D. J., Puls J., Lanz T., Martins F., 2006, A&A, 456, 659
Nota A., Pasquali A., Clampin M., Pollacco D., Scuderi S., Livio M., 1996, ApJ, 473, 946
Orlando S., Miceli M., Pumo M. L., Bocchino F., 2015, ApJ, 810, 168
Petermann E., Langer N., Castro N., Fossati L., 2015, A&A, 584, A54
Puebla R. E., Hillier D. J., Zsargo J., Cohen D. H., Leutenegger M. A., 2016, MNRAS, 456, 2907
Rousseau J., Martin N., Préévot L., Rebeirot E., Robin A., Brunet J. P., 1978, A&AS, 31, 243
Schneider F. R. N., Podsiadlowski P., Langer N., Castro N., Fossati L., 2016, MNRAS, 457, 2355
Searle S. C., Prinja R. K., Massa D., Ryans R., 2008, A&A, 481, 777
Smartt S. J., Lennon D. J., Kudritzki R. P., Rosales F., Ryans R. S. I., Wright N., 2002, A&A, 391, 979
Smith N., 2002, MNRAS, 331, 7
Smith N., 2007, AJ, 133, 1034
Smith N., 2014, ARA&A, 52, 487
Smith N., Townsend R. H. D., 2007, ApJ, 666, 967
Smith N., Bally J., Walawender J., 2007, AJ, 134, 846
Smith N., Li W., Silverman J. M., Ganeshalingam M., Filippenko A. V., 2011a, MNRAS, 415, 773
Smith N., Gehrz R. D., Campbell R., Kassis M., Le Mignant D., Kuluhiwa K., Filippenko A. V., 2011b, MNRAS, 418, 1959
Smith N., Arnett W. D., Bally J., Ginsburg A., Filippenko A. V., 2013, MNRAS, 429, 1324
Staveley-Smith L. et al., 1992, Nature, 355, 147
Staveley-Smith L., Briggs D. S., Rowe A. C. H., Manchester R. N., Reynolds J. E., Tzioumis A. K., Kesteven M. J., 1993, Nature, 366, 136
Taylor W. D., Evans C. J., Simon-Diaz S., Sana H., Langer N., Smith N., Smartt S. J., 2014, MNRAS, 442, 1483
Vink J. S., de Koter A., Lamers H. J. G. L. M., 2001, A&A, 369, 574
Walborn N. R., 1971, ApJS, 23, 257
Walborn N. R., Prevot M. L., Prevot L., Wamsteker W., Gonzalez R., Gilmozzi R., Fitzpatrick E. L., 1989, A&A, 219, 229
Zanardo G., Staveley-Smith L., Ng C. Y., Gaensler B. M., Potter T. M., Manchester R. N., Tzioumis A. K., 2013, ApJ, 767, 98
Zsargo J., Hillier D. J., Bouret J. C., Lanz T., Leutenegger M. A., Cohen D. A., 2008, ApJ, 685, L149

This paper has been typeset from a TEX/LATEX file prepared by the author.